Journal of Radioanalytical and Nuclear Chemistry (2019) 319:1119–1125
https://doi.org/10.1007/s10967-019-06434-8

^{131}I-labeled PEG and folic acid co-functionalized graphene quantum dots for tumor-targeted imaging

Yunhan Wang[1,2] · Hu Song[2] · Guanquan Wang[2] · Xia Yang[2] · Jing Wang[2] · Hongyuan Wei[1,2]

Received: 24 October 2018 / Published online: 30 January 2019

Abstract
In this study, we successfully synthesized polyethylene glycol (PEG) and folic acid (FA) co-functionalized graphene quantum dots (GQDs) to improve the biocompatibility and tumor-targeting ability of GQDs simultaneously, and labeled GQDs–PEG–FA with ^{131}I for biological behavior evaluation. The in vitro properties, biodistribution and SPECT imaging of ^{131}I-GQDs–PEG–FA were investigated. The uptake of ^{131}I-GQDs–PEG–FA at tumor sites can be clearly examined via SPECT imaging, which can ascribe to enhanced permeability and retention effect and active targeting effect of FA to folate receptors. The results indicate that ^{131}I-GQDs–PEG–FA can be used as a radioactive probe for detection of tumor cells overexpressing folate receptor.

Keywords Graphene quantum dots · Polyethylene glycol · Folic acid · Active targeting · Tumor · ^{131}I

Introduction

Graphene quantum dost (GQDs) are thought to be effective drug delivery carriers owing to their excellent physical and chemical properties [1–3]. Functionalization of GQDs can further increase their biocompatability [4, 5] or active targeting ability to tumor cells [6–10]. Chandra et al. [4] funtionalized GQDs with polyethylene glycol (PEG) showing lower cytotoxicity than prestine GQDs. Chong et al. [5] also found that there was no observable toxicity of PEG–GQDs on A549 cells and HeLa cells, and that PEG–GQDs had good biocompatibility in mice. Abdullah-Al-Nahain et al. [6] found that hyaluronic acid (HA) functionalized GQDs (HA–GQDs) showed effective targeting to A549 cells and HA–GQDs did not change the toxicity of GQDs. Folic acid (FA) modified GQDs increased the internalization in human cervical cancer Hela cells overexpressing folate receptors [7, 8]. GQDs conjugated monoclonal antibodies can target antigens on the surface of cancer cells via transmembrane receptors or cell growth factors [9, 10].

However, current studies usually focus on either biocompatibility or tumor-targeting ability. Besides, researchers always understake study in vitro. For biological application, it is necessary to consider improving the biocompatibility and tumor-targeting ability of GQDs at the same time [1]. In our previous studies, we have observed passive targeting of GQDs to tumors, which can contribute to enhanced permeability and retention (EPR) effect [11]. To make a further step, we synthesize PEG and folic acid co-functionalized GQDs to improve biocompatibility and tumor-targeting ability simultaneously in this paper. Then we labeled GQDs–PEG–FA with ^{131}I and investigated its in vitro and in vivo properties for biological behavior evaluation.

Experimental

General

Na^{131}I was supplied by Institute of Nuclear Phyics and Chemistry, China Academy of Engineering Physics. 3-(4,5-Dimethylthiazol-2-yl)-5-(3-carboxymethoxyphenyl)-2-(4-sulfophenyl)-2H-tetrazolium (MTS) Cell Proliferation Colorimetric Assay Kit was purchased from Sigma-aldrich. DMEM (Dulbecco's Modified Eagle Medium, high glucose)

✉ Hongyuan Wei
wwwhy@126.com

[1] Department of Nuclear Medicine, First Affiliated Hospital of Southwest Medical University, Luzhou 646000, People's Republic of China

[2] Institute of Nuclear Physics and Chemistry, China Academy of Engineering Physics, Mianyang 621999, People's Republic of China

cell culture medium, trypsin, penicillin, and streptomycin are purchased from Gibco Invitrogen. Iodogen (1,3,4,6-tetrachloro-3alpha,6alpha-diphenylglucoluril), DOX (Doxorubicin hydrochloride) and other chemical reagents were purchased from Aladdin Reagent Co., Ltd. Hela and HEK293 cell lines were purchased from Shanghai Cell Bank, Chinese Academy of Sciences.

UV–Vis measurement was conducted with a Lambda 850 spectrophotometer (Perkin Elmer). The Fourier transform infrared (FTIR) spectrum was obtained on a FT-IR spectrophotometer (Thermo Nicolet 360). The radioactivity count was carried out using an FJ-2021 γ radio-immune counter. SPECT imaging studies were performed on a GE Infinia Hawkeye4 SPECT, which was provided by First Affiliated Hospital of Southwest Medical University.

Preparation of GQDs–PEG–FA and ^{131}I-GQDs–PEG–FA

GQDs were prepared with a bottom-up method form citric acid and characterized as our previous work [11]. Co-functionalization of PEG and FA of GQDs was performed referring reported procedures [12]. An activated ester of FA, NHS–FA, was first synthesized. Briefly, FA (100 mg) was dissolved in 10 ml DMSO along with 1.1 molor excess NHS and DCC. The reaction mixture was stirred overnight in darkness at room temperature. After filtration of the insoluble byproduct, NHS–FA was got for further synthesis. FA–PEG–amine was then synthesized by reacting PEG diamine with equimolar NHS–FA in DMSO. The product was purified by gel-filtration on a Sephadex G-25 column equilibrated in deionized water. The FA–PEG-amine was eluted as a light yellow band. GQDs–PEG–FA was finally synthesized by reaction GQDs with FA–PEG-amine in the presence of EDC and NHS in water. GQDs–PEG–FA was purified by dialysis against deionized water. The synthesis route is schematic illustrated Fig. 1.

^{131}I-GQDs–PEG–FA was prepared by Iodogen method as the same procedure of our previous work [11]. Briefly, 0.2 ml GQDs–PEG–FA solution with the concentration of 20 mg/ml was transferred to 0.1 mg Iodogen coated tube and then 0.01 ml Na^{131}I (~ 3.7×10^7 Bq) solution was added. The tube was shaked for 10 min at room temperature to finish the iodination reaction. Finally, the labled product was separated from the tube. Quality control of labeling yield was determined by paper chromatography developed by acetonitrile.

In vitro properties of ^{131}I-GQDs–PEG–FA

The in vitro stability in saline and BSA and lipid-water partition coefficient of ^{131}I-GQDs–PEG–FA were evaluated. Aliquotes of ^{131}I-GQDs–PEG–FA solution (0.05 ml) were incubated with saline and BSA for 48 h at 37 °C. The radiochemical purity was analyzed by the same protocol for quality control. The in vitro stability can be evaluated according to the radiochemical purity. Partition coefficient was tested by ''shake-flask'' method using an FJ-2021 γ radio-immune counter [13].

Cytotoxicity assay

The in vitro cytotoxicity of GQDs–PEG–FA on Hela cells and HEK293 cells was performed by MTS cell proliferation colorimetric assay. Cells were seeded on 96-well culture plates with the density of about 5×10^3 cells/well and incubated overnight. The culture medium was replaced by new DMEM mixed 5% of GQDs–PEG–FA with various concentrations. DOX with the concentration of 10 μg/ml was used for positive control. Cells were incubated for further 24–48 h. The mixture culture medium was aspirated and cells were washed by PBS twice. Afterwards, cells were treated with 100 μl DMEM mixed 10% MTS solution and incubated for 4 h. The optical density value of each hole was determined at 490 nm.

Cell uptake of ^{131}I-GQDs–PEG–FA

Hela cells were seeded on 12-well culture plates with the density of about 3×10^5 cells/well and incubated overnight to allow the cells to attach on the plate. The culture media of three groups were replaced by new DMEM mixed 5% of ^{131}I-GQDs–PEG–FA (200 μg/ml, ~ 3.7×10^4 Bq), ^{131}I-GQDs (200 μg/ml, ~ 3.7×10^4 Bq) and ^{131}I-GQDs–PEG–FA (200 μg/ml, ~ 3.7×10^4 Bq) + FA (2 mM), respectively. Cells were incubated for further 4 h. The mixture culture medium was aspirated and cells were washed by PBS twice. Afterwards, the plate was treated with 500 μl 1 M NaOH to detach the cells and then washed by 1 M NaOH. All solution containing NaOH and cells was collected in immunecounting tube and was detected for radiocounting by a FJ-2021 γ counter.

Biodistribution of ^{131}I-GQDs–PEG–FA in normal mice

All animal experiments were performed according to the guidelines and protocols approved by the Animal Investigation Committee of Southwest Medical University (The ethic number is 20171112131). Normal Kunming (KM) mice were intravenously injected ^{131}I-GQDs–PEG–FA (0.1 ml, ~ 3.7×10^5 Bq) via the tail. Various tissues (blood, heart, liver, spleen, lung, kidney, muscle and intestine) of each group at different time points post injection were excised, weighted, and measured for raidoactivity. The radioactivity data were corrected for physical decay.

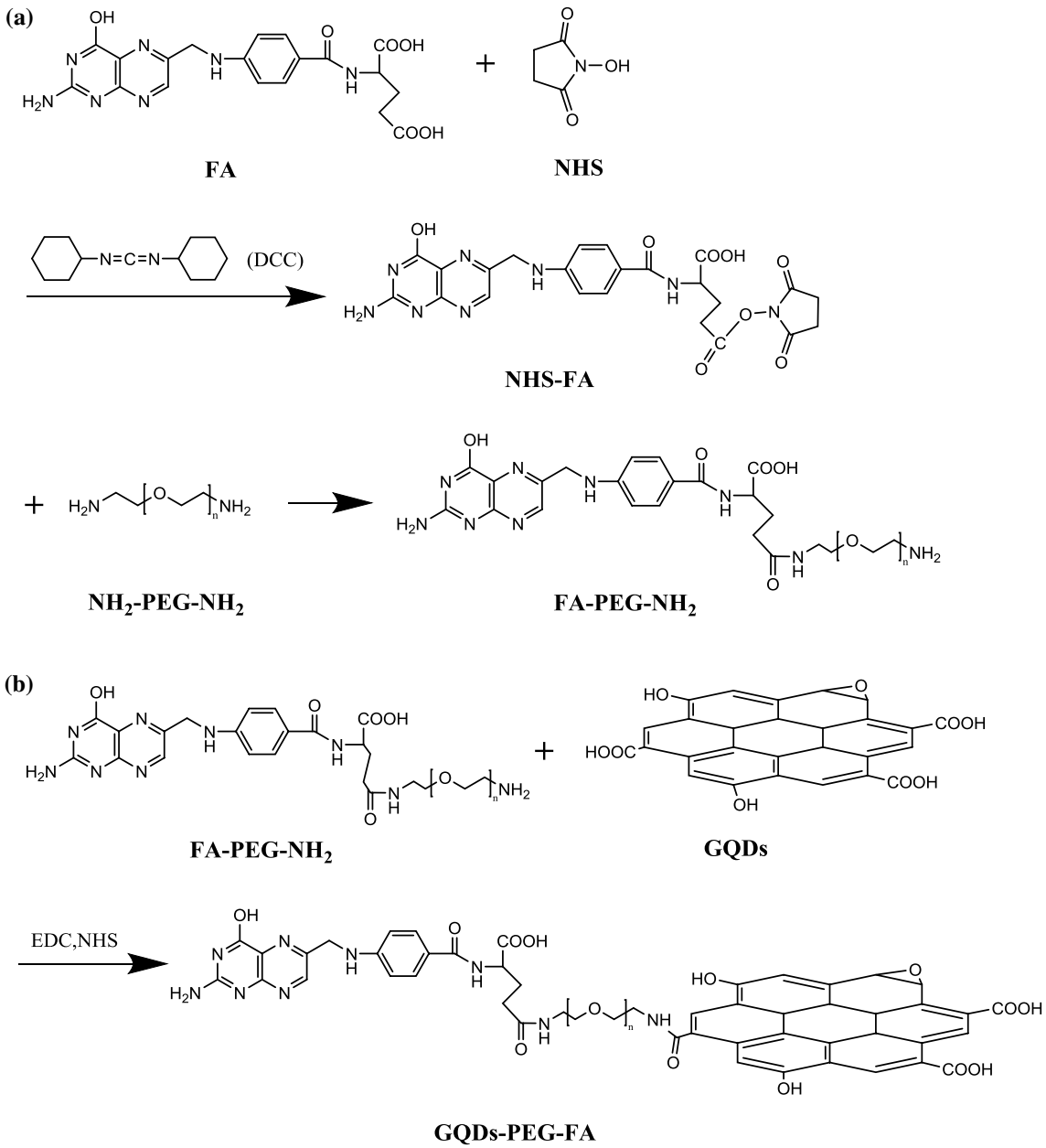

Fig. 1 Synthesis of FA–PEG-amine (**a**) and GQDs–PEG–FA (**b**)

Xenograft tumor model

All animal experiments were performed according to the guidelines and protocols approved by the Animal Investigation Committee of Southwest Medical University (The ethic number is 20171112131). Female BALB/c nude mice (20 ± 2 g, SPF grade) were purchased from Chengdu Dashuo Biotechnology Company. About 1.0×10^7 suspension Hela cells in 0.1 ml PBS were injected subcutaneously at the right shoulder of the nude mice. After about 21 days housing, tumor models of near size (1.5 ± 0.2 cm) diameter were employed.

SPECT imaging of ^{131}I-GQDs–PEG–FA in tumor bearing mice

Before SPECT imaging experiment, the tumor bearing mice were administrated with potassium iodide solution (0.5%) for three days to saturate the thyroid. After that, two group tumor bearing mice (two mice each group) were intravenously injected ^{131}I-GQDs–PEG–FA (0.1 ml, ~ 3.7×10^6 Bq) and whole-body SPECT imaging was performed at 8 h and 24 h post injection, respectively. Then the mice were sacrificed and tumor, blood and muscle were excised, weighted, and measured for raidoactivity. Blocking studies were also

taken to identify the specific binding of ^{131}I-GQDs–PEG–FA to folate receptors in the tumor. Tumor bearing mice were administrated with potassium iodide solution (0.5%) for 3 days ad libitum, and were fed FA for 3 days (3 times per day, 0.5 mg each time) before SPECT imaging. The mice were intravenously injected ^{131}I-GQDs–PEG–FA (0.1 ml, ~ 3.7×10^6 Bq) and were performed SPECT imaging study at the same time points post injection.

Results and discussion

Characterization of GQDs–PEG–FA and ^{131}I-GQDs–PEG–FA

The UV–Vis spectrum of GQDs–PEG–FA is shown in Fig. 2. Compared with GQDs, absorbance intensity at 360 nm of GQDs–PEG–FA dramatically decreased. The FTIR spectra of GQDs–PEG–FA, GQDs and PEG–FA are shown in Fig. 3. The spectrum of GQDs–PEG–FA clearly shows the prescene of C–N (~ 1250 cm^{-1}), CO–NH (~ 1643 cm^{-1}), CH_2 (~ 2910 cm^{-1}) and NH (~ 3200 cm^{-1}) functional groups, indicating successful conjugation of GQDs and PEG–FA by amide bond. The TLC radio-spectra of ^{131}I-GQDs–PEG–FA and free ^{131}I are illustrated in Fig. 4. The R_f values of ^{131}I-GQDs–PEG–FA and free ^{131}I ion are 0.1–0.03 and 0.9–1.0, respectively. The results indicate high labeling yield of ^{131}I-GQDs–PEG–FA.

In vitro properties of ^{131}I-GQDs–PEG–FA

The radiochemical purity of ^{131}I-GQDs–PEG–FA was 87% and 85% in saline and BSA at 48 h, respectively. It is almost the same with ^{131}I-GQDs [11], which shows the conjugation of PEG–FA did not make a difference in ^{131}I labeling.

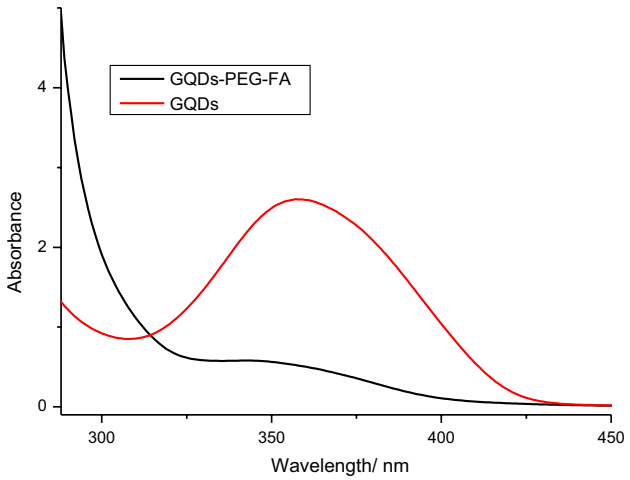

Fig. 2 UV–Vis spectrum of GQDs–PEG–FA

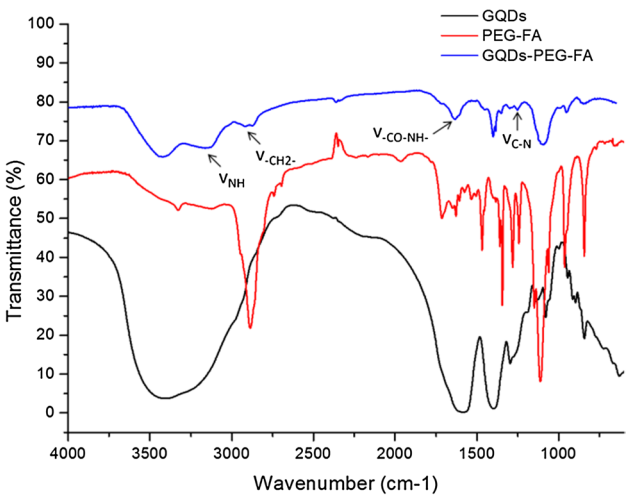

Fig. 3 FTIR spectra of GQDs–PEG–FA, GQDs and PEG–FA

The partition coefficient of ^{131}I-GQDs–PEG–FA (logPo/w) was -1.534 ± 0.005. By comparison with ^{131}I-GQDs [11], ^{131}I-GQDs–PEG–FA becomes even more hydrophilic, which should be the result of high water solubility of PEG.

Cytotoxicity

The in vitro cytotoxicity results of GQDs–PEG–FA to Hela cells and HEK293 cells were shown in Fig. 5, showing that the cell viability of GQDs–PEG–FA with the concentration of 100 μg/ml at 48 h to Hela cells and HEK293 cells was 95% and 93%, respectively. GQDs–PEG–FA shows better biocompatibility compared with GQDs [11]. This is in line with our expectation that PEG may improve the biocompatability. In other hands, for the low cytotoxicity of GQDs–PEG–FA, the amount of ^{131}I-GQDs–PEG–FA used for biodistribution and SPECT imaging study was safe for experimental animals.

Cell uptake of ^{131}I-GQDs–PEG–FA

Figure 6 shows Hela cell uptake results of ^{131}I-GQDs, ^{131}I-GQDs–PEG–FA and ^{131}I-GQDs–PEG–FA + FA. The uptake of ^{131}I-GQDs–PEG–FA by Hela cells is significantly higher than that of ^{131}I-GQDs and ^{131}I-GQDs–PEG–FA + FA. The radioactivity count of ^{131}I-GQDs–PEG–FA containing free folic acid is almost the same as that of ^{131}I-GQDs. This may be result of that free folic acid binds preferentially to folate receptors of Hela cells and co-incubation of folic acid and ^{131}I-GQDs–PEG–FA forms blocking effect to folate receptors [8]. The results indicate the interaction between ^{131}I-GQDs–PEG–FA and folate receptor could significantly promote cell uptake.

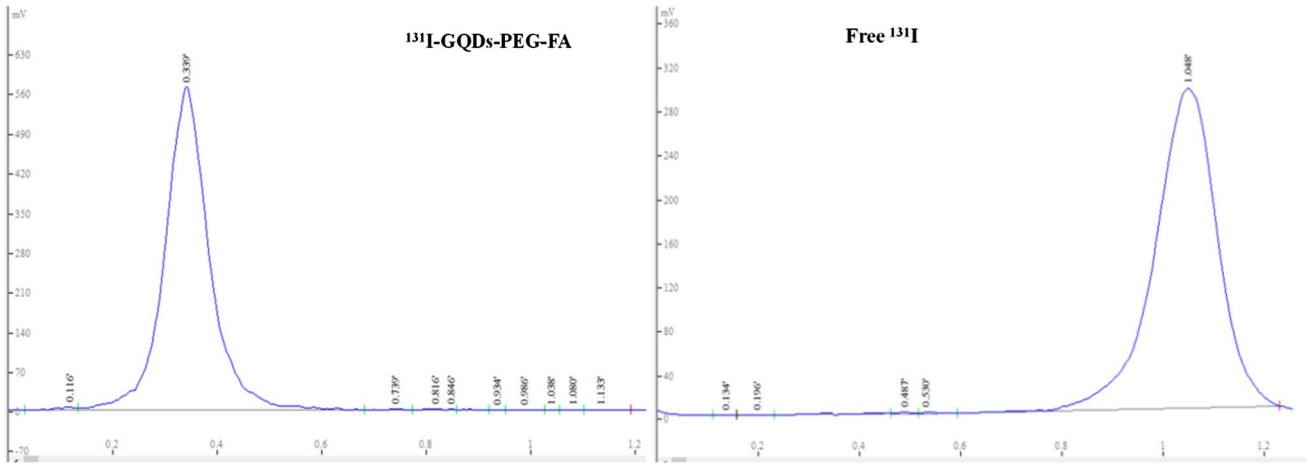

Fig. 4 TLC raido-spectra of ^{131}I-GQDs–PEG–FA and free ^{131}I

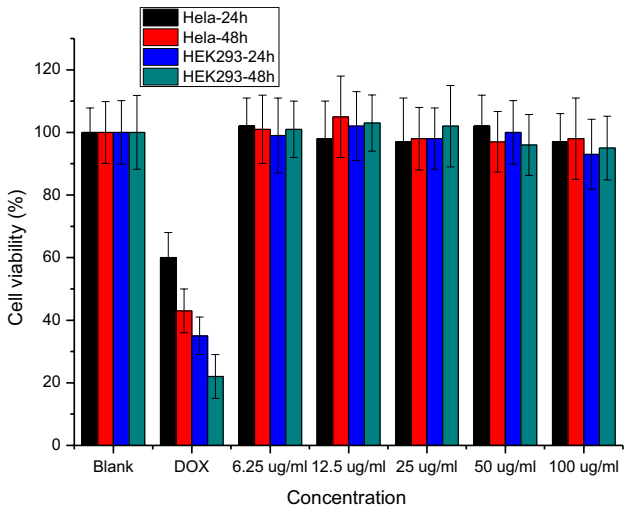

Fig. 5 *In vitro* cytotoxicity of GQDs–PEG–FA to Hela cells and HEK293 cells (Data represent mean ± SD, n = 5)

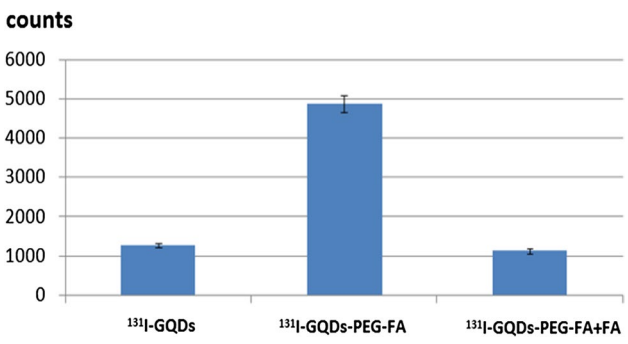

Fig. 6 Hela cell uptake of ^{131}I-GQDs, ^{131}I-GQDs–PEG–FA and ^{131}I-GQDs–PEG–FA + FA (Data represent mean ± SD, n = 4)

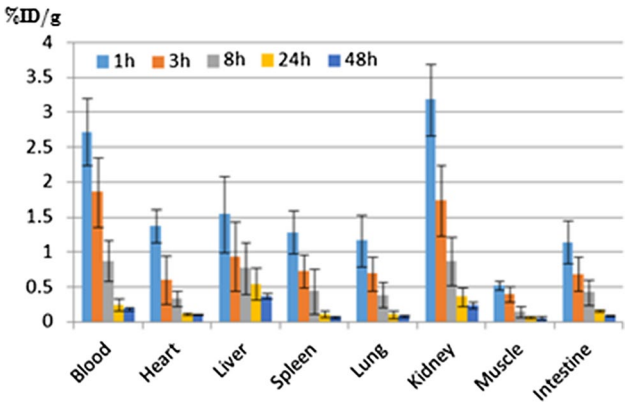

Fig. 7 In vivo biodistribution of ^{131}I-GQDs–PEG–FA in normal KM mice (Data represent mean ± SD, n = 4)

Biodistribution of ^{131}I-GQDs–PEG–FA

The biodistribution results of ^{131}I-GQDs–PEG–FA in normal KM mice were summarized in Fig. 7. The data present that ^{131}I-GQDs–PEG–FA has similar biodistribution behavior with ^{131}I-GQDs [11]. At 1 h post injection, all selected tissues have high radioactive uptakes, indicating that ^{131}I-GQDs–PEG–FA has fast distribution. At 48 h post injection, the radioactivity decreased to a very low level, which means ^{131}I-GQDs–PEG–FA has rapid clearance. The kidney has the highest radioactive uptake compared with other organs at 1 h, 3 h and 8 h post injection, suggesting that ^{131}I-GQDs–PEG–FA was mainly metabolized by kidney. Comparatively high uptake in liver and spleen indicates that mononuclear phagocyte system also plays an important role in clearing nanosized ^{131}I-GQDs–PEG–FA [11, 13].

SPECT imaging of ^{131}I-GQDs–PEG–FA

The SPECT images of ^{131}I-GQDs–PEG–FA and ^{131}I-GQDs–PEG–FA + blocking in tumor bearing mice at 8 h and 24 h are shown in Fig. 8. The highest radioactive uptakes in bladder were observed in both ^{131}I-GQDs–PEG–FA and ^{131}I-GQDs–PEG–FA + blocking, which confirmed that ^{131}I-GQDs–PEG–FA was mainly metabolized by kidney.

In ^{131}I-GQDs–PEG–FA images, the radioactive uptakes in liver and tumor have a high level. The high uptakes in liver comfirmed that mononuclear phagocyte system had important role in clearing ^{131}I-GQDs–PEG–FA. Besides, the uptakes in tumor can be clearly examined, which is of the most interest. In ^{131}I-GQDs–PEG–FA + blocking images, the radioactive uptake in liver is high. However, the uptakes in tumor is not as clear as ^{131}I-GQDs–PEG–FA images, which is similar to ^{131}I-GQDs [11]. The results conform the specific binding of ^{131}I-GQDs–PEG–FA to folate receptors in the tumor.

In order to obtain quantitative results, we dissected the tumor bearing mice injected ^{131}I-GQDs–PEG–FA and measured their blood, muscle and tumor distribution data. The ID %/g of tumor was 2.82 and 1.94 at 8 h and 24 h post injection, respectively. T/B ratios are 2.43 and 2.67 at 8 h and 24 h, respectively. T/M ratios are 5.98 and 6.27 at 8 h and 24 h, respectively. Compared with ^{131}I-GQDs (T/B ratios are 0.77, 0.94 and 1.76 at 1 h, 3 h and 24 h, respectively. T/M ratios are 2.15, 2.68, and 3.47 at 1 h, 3 h and 24 h) [11], T/B and T/M of ^{131}I-GQDs–PEG–FA are significantly higher. The active targeting effect of FA to folate receptors of tumors can be responsible for the uptake enhancement in tumor. As illustrated in Fig. 9, except for EPR effect [11, 14–16], ^{131}I-GQDs–PEG–FA can actively target tumor cells owing to the interaction of FA and folate receptor [7, 8, 17–20] after permeating the vascular endothelium of tumor tissues, resulting in higher uptake at tumor site.

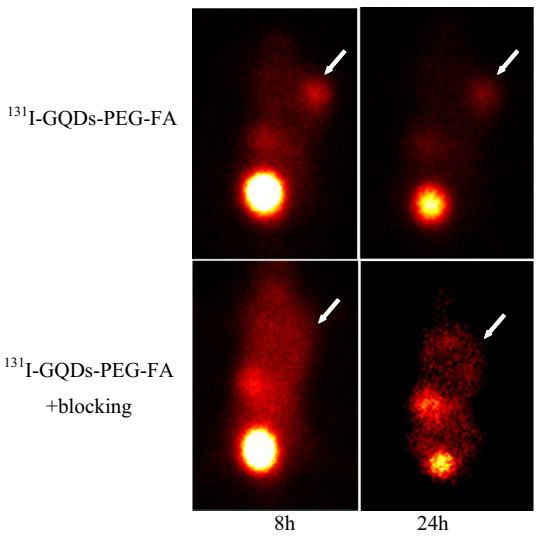

Fig. 8 SPECT images of ^{131}I-GQDs–PEG–FA and ^{131}I-GQDs–PEG–FA + blocking in tumor bearing mice (The arrows point at tumor sites.)

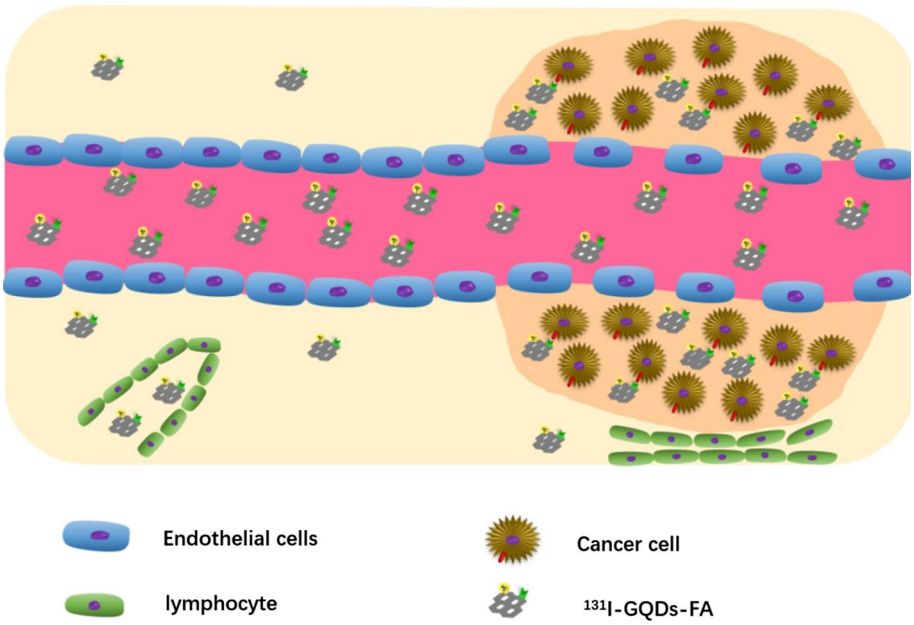

Fig. 9 Schematic illustration of targeting effect to tumors of ^{131}I-GQDs–PEG–FA

Conclusions

In this study, we successfully synthesized PEG and folic acid co-functionalized graphene quantum dots, and labeled it with ^{131}I for biological behavior evaluation. GQDs-PEG-FA shows low cytotoxicity and high biocompatibility. ^{131}I-GQDs–PEG–FA is of good in vitro stability and hydrophilic. By intravenously injected via the tail to normal KM mice, ^{131}I-GQDs–PEG–FA is fast distributed to tissues and rapidly metabolized over 48 h post injection. ^{131}I-GQDs–PEG–FA mainly excretes through urine and the liver plays an important part in cleaning ^{131}I-GQDs–PEG–FA. By intravenously injected via the tail to tumor bearing mice, the uptake of ^{131}I-GQDs–PEG–FA at tumor sites can be clearly examined via SPECT imaging. T/B value and T/M value of ^{131}I-GQDs–PEG–FA are significantly higher than ^{131}I-GQDs, which can contribute to the active targeting effect of FA to folate receptors. The results indicate that ^{131}I-GQDs–PEG–FA can be used as a radioactive probe for detection of tumor cells overexpressing folate receptor.

Acknowledgements This work was financially supported by the National Nature Science Foundation of China (NSFC-21471138, NSFC-21401176).

Compliance with ethical standards

Conflict of interest The authors of the manuscript declare that there is no conflict of interest.

References

1. Schroeder KL, Goreham RV, Nann T (2016) Graphene quantum dots for theranostics and bioimaging. Pharm Res 33:2337–2357
2. Zheng XT, Ananthanarayanan A, Luo KQ, Chen P (2015) Glowing graphene quantum dots and carbon dots: properties, syntheses, and biological applications. Small 11:1620–1636
3. Iannazzo D, Pistone A, Salamo M, Galvagno S, Romeo R, Giofre SV, Branca C, Visalli G, Di Pietro A (2017) Graphene quantum dots for cancer targeted drug delivery. Int J Pharm 518:185–192
4. Chandra A, Deshpande S, Shinde DB, Pillai VK, Singh N (2014) Mitigating the cytotoxicity of graphene quantum dots and enhancing their applications in bioimaging and drug delivery. ACS Macro Lett 3:1064–1068
5. Chong Y, Ma Y, Shen H, Tu X, Zhou X, Xu J, Dai J, Fan S, Zhang Z (2014) The in vitro and in vivo toxicity of graphene quantum dots. Biomaterials 35:5041–5048
6. Abdullah Al N, Lee JE, In I, Lee H, Lee KD, Jeong JH, Park SY (2013) Target delivery and cell imaging using hyaluronic acid-functionalized graphene quantum dots. Mol Pharm 10:3736–3744
7. Huang CL, Huang CC, Mai FD, Yen CL, Tzing SH, Hsieh HT, Ling YC, Chang JY (2015) Application of paramagnetic graphene quantum dots as a platform for simultaneous dual-modality bioimaging and tumor-targeted drug delivery. J Mater Chem B 3:651–664
8. Wang X, Sun X, Lao J, He H, Cheng T, Wang M, Wang S, Huang F (2014) Multifunctional graphene quantum dots for simultaneous targeted cellular imaging and drug delivery. Colloid Surface B 122:638–644
9. Zou F, Zhou H, Tan TV, Kim J, Koh K, Lee J (2015) Dual-mode SERS-fluorescence immunoassay using graphene quantum dot labeling on one-dimensional aligned magnetoplasmonic nanoparticles. ACS Appl Mater Int 7:12168–12175
10. Zheng XT, He HL, Li CM (2013) Multifunctional graphene quantum dots-conjugated titanate nanoflowers for fluorescence-trackable targeted drug delivery. RSC Adv 3:24853–24857
11. Song H, Wang YH, Wang J, Wang GQ, He JH, Wei HY, Luo SZ (2018) Prepartion and biodistribution of ^{131}I-labeled graphene quantum dots. J Radioanal Nucl Chem 316:685–690
12. Guo W, Lee RJ (1999) Receptor-targeted gene delivery viafolate-conjugated polyethylenimine. AAPS Pharmsci 1:20–26
13. Song H, Luo SZ, Wei HY, Song HT, Yang YQ, Zhao WW (2010) In vivo biological behavior of ^{99m}Tc(CO)$_3$ labeled fullerol. J Radioanal Nucl Chem 285:635–639
14. Maeda H (2012) Macromolecular therapeutics in cancer treatment: the EPR effect and beyond. J Control Rel 164:138–144
15. Maeda H, Matsumura Y (2011) EPR effect based drug design and clinical outlook for enhanced cancer chemotherapy. Adv Drug Deliv Rev 63:129–130
16. Maeda H, Nakamura H, Fang J (2013) The EPR effect for macromolecular drug delivery to solid tumors: improvement of tumor uptake, lowering of systemic toxicity, and distinct tumor imaging in vivo. Adv Drug Deliv Rev 65:71–79
17. Zhang RY, Wang ZY, Yang XQ, Xuan Y, Cheng K, Li C, Song XL, An J, Hou XL, Zhao YD (2017) Folic acid modified Pluronic F127 coating Ag_2S quantum dot for photoacoustic imaging of tumor cell-targeting. Nanotechnology. 29:055101
18. Tian Y, Li JC, Zhu JX, Zhu N, Zhang HM, Liang L, Sun L (2017) Folic acid-targeted etoposide cubosomes for theranostic application of cancer cell imaging and therapy. Med Sci Monit 23:2426–2435
19. Hai X, Wang YT, Hao XY, Chen XW, Wang JH (2018) Folic acid encapsulated graphene quantum dots for ratiometric pH sensing and specific multicolor imaging in living cells. Sens Actuat B Chem 268:61–69
20. Lin JY, Hu WW, Gao FL, Qin JB, Cheng P, Lu XW (2018) Folic acid-modified diatrizoic acid-linked dendrimer-entrapped gold nanoparticles enable targeted CT imaging of human cervical cancer. J Cancer 9:564–577